Applied Energy 334 (2023) 120715

Contents lists available at ScienceDirect

Applied Energy

journal homepage: www.elsevier.com/locate/apenergy

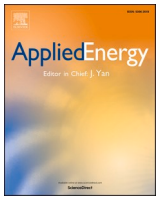

Ultra-low frequency multidirectional harvester for wind turbines

Carlos Castellano-Aldave [a], Alfonso Carlosena [a,c,*], Xabier Iriarte [b,c], Aitor Plaza [b]

[a] Department of Electrical, Electronic and Communications Engineering, Public University of Navarre, Arrosadía Campus 31006, Pamplona, Spain
[b] Department of Engineering, Public University of Navarre, Arrosadía Campus 31006, Pamplona, Spain
[c] Institute of Smart Cities (ISC), Public University of Navarre, Arrosadía Campus 31006, Pamplona, Spain

HIGHLIGHTS

- A novel ultra-low frequency (down to 0.3 Hz), low acceleration (<1 g) and multidirectional vibration-based harvester is proposed.
- The device has been designed for the conditions of a wind turbine. However it could be used in other vibrating system with similar specs.
- The device is non-resonant, multidirectional (on a plane), and based on mechanical to electrical conversion through EM coupling.
- A prototype has been fabricated, modelled and thoroughly tested. Numerical simulations agree with experimental results.
- The device can generate a few mW at frequencies around 1 Hz @ 50 mm. (e.g. 9.3 mW at 1.2 Hz with 0.3 g accelerations).

ARTICLE INFO

Keywords:
Energy Harvesting
Vibration-to-Electrical Energy Conversion
Electromagnetic Transduction
Ultra-low frequency
Autonomous Sensors
Wind Turbines

ABSTRACT

In this paper we propose, and demonstrate through a prototype, a completely novel device able to harvest mechanical energy from the multidirectional vibrations in a wind turbine, and convert it into electrical, to power autonomous sensors. The application is very challenging since vibrations are of ultra-low frequency, well below 1 Hz, with accelerations of tenths of cm/s^2 (0.01 g), and the device must capture energy from the movement in any direction. According to our experiments, the device is capable to generate average powers around the milliwatt in the operation conditions of a wind turbine, which are enough for some very-low power sensor nodes, or at least to considerably extend the life-time of batteries. The device is based on the principle of moving (inertial) masses comprised of magnets in Hallbach arrays interacting with coils, and can work for movements on any direction of a plane. To the best of our knowledge, this is the first device specifically proposed for wind turbines and one of the few that work in such low frequencies, and capture energy from movements on any direction on a plane. Only three harvesters proposed in the literature, intended for distinct applications, can work at such low frequencies, and our device exhibits a better efficiency. Though comparisons with harvesters working in different contexts and, even using different conversion principles, is not completely fair, we make in this paper a comparison to the closest ones, resorting to two different figures of merit.

1. Introduction

Energy harvesting (EH) from ambient sources has been a topic of intense research in the last twenty years. The main goal is to have available autonomous devices which do not require either wired power sources, or periodic maintenance to recharge or replace batteries. The idea can be traced back to the popular in the old days' crystal radio, where the electromagnetic signal carrying the information was also used to power the device. Today, the need to deploy a plethora of devices, mainly sensors, together with the concerns on the energy waste and cost of maintenance, are the driving forces for the research in the area.

EH is on its own merits a multidisciplinary topic where energy sources, sensing and conversion principles, materials, mechanical designs and electronics converge. Therefore, it is almost impossible to have a comprehensive and unified picture of the field. Apart from some books or tutorial papers which unavoidably have a compilation character [1,2], literature is plagued with papers that try to solve a particular problem oriented to a given application. Thus, it is not possible, and

* Corresponding author at: Dpt. Electrical, Electronic and Communications Engineering, Public University of Navarre, Campus de Arrosadia, E31006 Pamplona, Spain.
E-mail addresses: carlos.castellano@unavarra.es (C. Castellano-Aldave), alfonso.carlosena@unavarra.es (A. Carlosena), xabier.iriarte@unavarra.es (X. Iriarte), aitor.plaza@unavarra.es (A. Plaza).

https://doi.org/10.1016/j.apenergy.2023.120715
Received 7 June 2022; Received in revised form 30 December 2022; Accepted 16 January 2023
Available online 24 January 2023

even does not make much sense, to try to compare different designs and decide which is best even for akin applications.

In this paper we will mainly focus on an application which has received so far limited attention, in spite of its growing interest. We refer, broadly speaking, to Condition Monitoring (CM) or Structural Health Monitoring (SHM) of wind turbines [3,4]. There is a current trend to extend, when possible, the operating life of wind parks which were installed many years ago. This requires a continuous monitoring of some parameters, remarkably accelerations, at different points of the tower and nacelle to calculate the mechanical parameters of the structure, determine its condition, and estimate the remaining life-time.

However, not only already installed, and old, wind parks need to be sensorized, but also new on-shore and off-shore parks must include complete monitoring systems to predict possible failures and analyze the evolution of the structures [5]. The need for monitoring extends also to the process of tower construction, where wind effects (e.g. vortex shedding) may produce early damages in the structure which are not easily detected. Transportation of blades or tower sections is another source of damages. Energy for powering is not directly available in those cases, and the use of completely autonomous devices in terms of energy, which can also wirelessly communicate with a host, are highly desirable for installation and maintenance purposes anyway.

In wind turbines, the most readily available source of energy is the mechanical movement, i.e. vibration, of the structure which is, obviously, particularly relevant under operating conditions. However, vibrations present are random in nature and of very low frequency, with also low levels of accelerations. Such accelerations are thus unpredictable in both intensity and directions, since the structure orientates in the wind direction, where vibrations are stronger. Regarding vibration frequencies, they cover a frequency band which is mainly dominated by the tower first mode (Typically between 0.3 and 0.5 Hz), and harmonics originated by the rotating frequency (named as 1P) and the blade passing frequency (3P), typically around 0.2 Hz and 0.6 Hz respectively for a tower around 100 m tall.

To cut it short, for the highest towers in the range of a few Megawatts, we are talking of frequencies below 1 Hz, accelerations up to 50 cm/s^2, and movement on any direction of a horizontal plane (XY) of a few cm [6]. Frequencies reduce as the tower size increases, as it is the case in off-shore structures. The excitation also contains energy at higher frequencies mainly due to the tower second mode (between 1 and 2 Hz), though they contribute less to produce energy. Taking this into account, the application at hand shares some specifications with others so distinct as human movement or ocean wave oscillations [7–12], that also belong to the so called “macroscale” applications [13]. In this scenario, almost all solutions are based on the kinetic to electrical conversions [14,15], which are mostly based on the Faraday principle, i.e., the generation of electricity that results from the relative movement of a coil in a magnetic field generated by a magnet [16].

For higher frequencies, and smaller devices, i.e. “microscale”, energy conversion based on the piezoelectric or triboelectric effects is the dominant. In the first case, piezoelectric devices are designed to tune their resonance(s) with the dominant vibration frequencies. Therefore, as frequency decreases, there are also combined solutions where two or more transduction mechanisms are combined [17–19] and/or natural low frequencies are multiplied or upscaled by mechanical devices to allow for piezoelectric devices [20–22].

The design of energy harvesters for ultralow frequencies is still an open problem which has been scarcely treated [23,24]. We should note here that the term ultra-low is not precisely defined, referring in most case to vibrations of “a few” hertz, or below 10 Hz [25–27]. In our case, we will consider even lower frequencies “around” and below 1 Hz, which is a much more challenging specification. We have identified only three papers showing results below 1 Hz, namely [10,23,28], but only the latter can work in multiple directions. There is another paper describing a two-directional device, which works at 2.6 Hz [26]. Last, in [29], authors propose a nonlinear device which harvests energy from vibrations between 0.5 and 5 Hz. However, the primary movement is a rotation (car wheel), and the device converts it into vibration. Moreover, experimental results are given for a reduced range from 1.5 to 4 Hz.

Therefore, in this paper we propose a novel solution for an unsolved problem, demonstrating a device that can work at frequencies below 1 Hz for arbitrary motions on a plane, which finds application in wind towers, and also in other civil structures, with the potential of providing power for autonomous sensor nodes, or to considerably extend the life-time of batteries.

The organization of the paper is as follows: in Section 2 we describe a prototype and its working principle, in order to give an intuitive insight to the harvester. Section 3 is devoted to model the device with a set of differential equations. In Section 4 we validate the model with some experimental results and identify the most relevant parameters, which are difficult to know a priori. Section 5 is devoted to analyzing the results given by the model under several conditions (transient, stationary and real excitations), always in the expected range of operation and to compare them with the experimental results. Maximum achievable power is then estimated and compared with the experimentally obtained values. In Section 6 our device is benchmarked against other state of the art harvesters. Section 7 is a summary of the main conclusions and future developments of our work.

2. Device description and motivation

Energy scavenging from vibration is mainly based on the use of an inertial mechanism, comprising a proof mass within a host case, which moves attached to the moving structure. This is shown in Fig. 1(a). The case is mounted on the moving structure and the proof mass, m, oscillates with respect to the casing-structure, when the structure vibrates in the direction of the device. The damping effect deliberately introduced, acting on the proof mass, is the mechanism for energy conversion, i.e., transduction. There is always a parasitic damping, due to friction, which needs to be minimized. Damping can either be proportional to velocity, as it is the case of electromagnetic conversion, or to the so-called Coulomb damping, which is typical of piezoelectric devices [15].

The behavior of inertial generators is quite different for high and low frequencies. The frontier region is mainly determined by the point where dimensions of the harvester device are close to oscillation amplitudes. At high frequencies with also high accelerations, device dimensions surpass oscillation amplitudes, whereas at low frequencies of operation the opposite is true. In the first case, movement range of the proof mass is lower than the device dimension, whereas in the second case such movement is clamped by the limitations of the device [30]. This is the reason why high frequency harvesters are designed to operate around their resonance frequency and are thus mostly based on piezoelectric conversion.

On the contrary, low frequency harvesters do not exploit resonance [27] and simply need to accommodate as much as possible the displacement of the proof mass to the device dimensions and thus to the displacement of the structure. Rotational devices, which convert linear movement into circular, have been proposed to circumvent these limitations, though it has been shown that they do not achieve any significant improvement with respect to linear ones [30]. Electromagnetic transduction is in any case the preferred conversion mechanism, which is coherent with the fact that piezoelectric devices cannot operate at very low frequencies. The proof mass usually consists of a combination of magnets, and the casing houses a number of coils. Their relative displacement induced by the vibration generates an electrical signal, following the Faraday’s law. This direct application of the electromagnetic conversion should not be confused with some sort of frequency up-conversion mechanism which combine magnetic interaction between magnets, to generate a lock/release mechanism to pluck piezoelectric cantilevers at their resonance frequency [22,31].

In the application at hand, wind turbines with power rates between 1 and 5 MW, tower tip or nacelle displacement can be up to $\pm$ 10 cm.

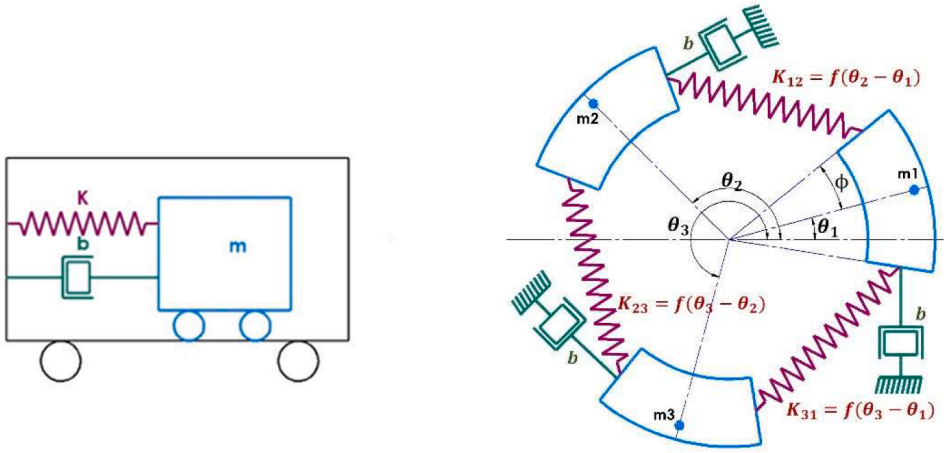

Fig. 1. Mass-spring-damper model a) linear b) circular with three masses and nonlinear stiffness.

Energy concentrates in a range of few hertz, dominated by tower first modes and harmonics generated by the rotation, which are typically below 1 Hz [6], though there is available power up to 2 Hz. Movement can be in any direction on a horizontal plane, depending obviously on the wind direction, and thus the conventional linear inertial mechanism in Fig. 1(a) would only work when aligned with the wind direction. This is the reason why we propose an inertial mechanism with three masses as schematically depicted in Fig. 1(b). Masses can freely rotate around a common axis which is fixed to a cylindrical casing. The three masses are evenly separated under repose conditions. Regardless of the movement direction, there will always be at least two masses that will angularly move with respect to the casing. Note that this is not a linear to rotation conversion since, in general, masses do not make a complete turn but just make angular oscillations in a limited range as we will show in the next sections.

The designed prototype, according to this idea, is shown in Fig. 2. It consists of a cylindrical case with a central axis. Picture on the left corresponds to the plane of movement, perpendicular to the axis of the cylinder. The three independent inertial proof masses, in black, can be guessed through the triangular windows. The base of the device, shown in the picture on the right, has an attached PCB where the basic circuitry for power conversion is included. A detailed 3D view of the three masses attached to the common rotation axis is shown in Fig. 3(a) In the prototype the masses are attached to the axis through low friction bearings.

Each mass contains an embedded array of magnets in a Halbach configuration [32,33], as shown in Fig. 3(b). Such configuration is known to concentrate the magnetic field, in this case at the external (convex) side of the blades. A positive by-side effect of the configuration is that the residual magnetic field on the sides is always outgoing, producing a repulsion between adjacent blades. The repulsive effect created between the sides of adjacent masses acts as a non-linear stiffness which tries to bring back the masses to their equilibrium position (evenly distributed at 120°), and reduces the impacts between them. When the device is shaken, at least two masses move regardless of the movement direction.

Fig. 4 shows images with numerical simulations of the magnetic field generated by the magnets in the Halbach array configuration. The concentration across the external sides is evident, in the same way a residual magnetic field remains in the lateral edges. The value of the magnetic across the red dashed line, 1 mm away from the magnets where coils are placed, is also depicted.

The case contains in its internal curved side an array of twenty-four coils, as shown in Fig. 5(a). Each coil is detailed in Fig. 5(b). The interaction between the moving magnets and the coils generates a voltage at the coil terminals, which are in turn used to generate the required power by combining all coils. Every set of magnets faces at least three complete coils, independently of its position, as shown in Fig. 5(c).

External device dimensions are 10 cm diameter and 9 cm height for the case. Mass of each blade is 0.158 Kg, which is mainly concentrated in the magnets, the radius to the center of masses being 3.7 cm. Total weight is 0.612 Kg. Other relevant dimensions are shown in Fig. 6. Note that device dimensions are of the order of the expected limits of the external movement. In this way, we can expect that blades can move, under optimal conditions, along its full dynamic range. We recall that this is not a rotating device, as described in [30]. The proposed geometry is intended to be capable of producing energy for movements on any direction of a plane, but not to generate it by continuous rotations of the masses around the axis but rather by back and forth motions, much in

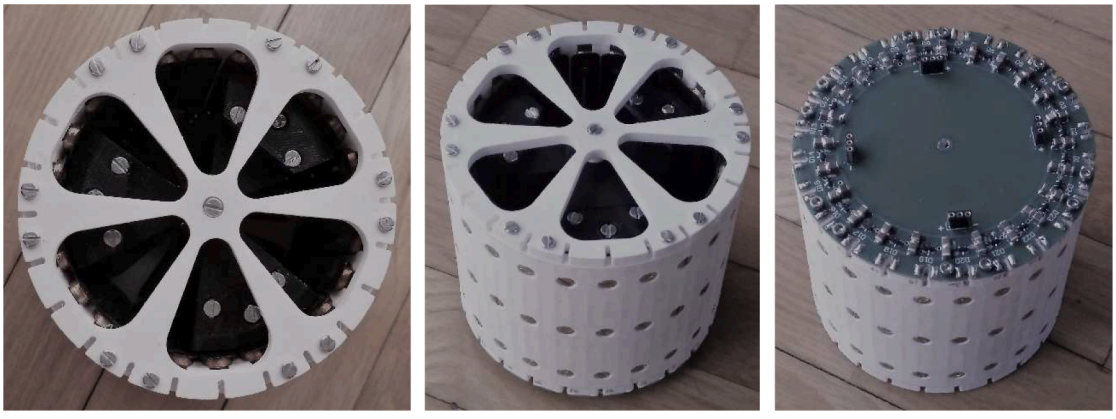

Fig. 2. Harvester prototype. Three different views.

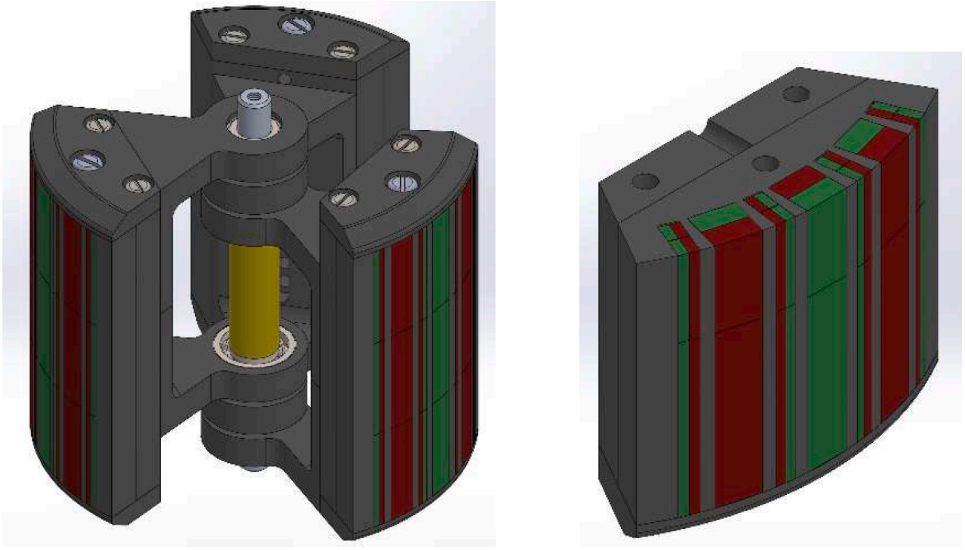

Fig. 3. (a) and (b). Different views of the moving masses with the Halbach arrays.

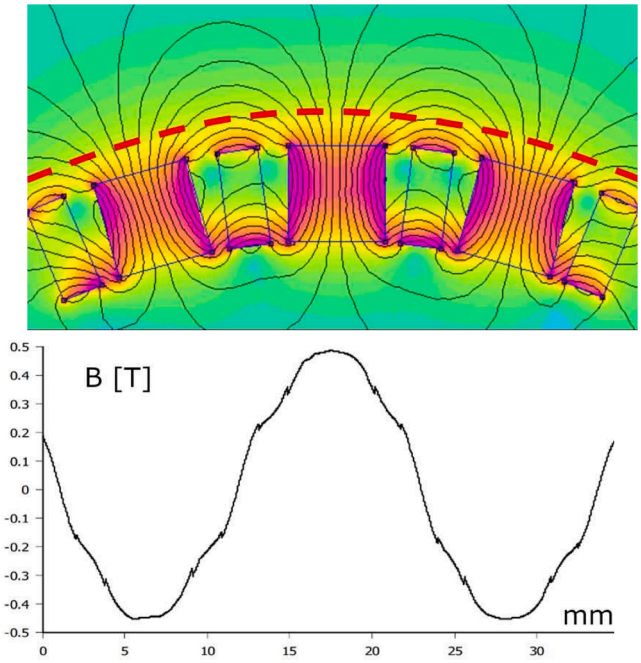

Fig. 4. Lines of magnetic field created by the magnets, and intensity at dashed line.

the same way as the harvester proposed in [34]. These are the conditions present in a wind turbine.

The prototype of the proposed device, shown in Fig. 2, has been fabricated and tested. Case and inertial masses chassis are made of ABS plastic and fabricated with a 3D printer. Each Halbach array consists of 9 magnets of 20x5x5mm and 12 magnets of 20x5x2mm. The coils are composed of 600 turns of enameled copper wire of 0.1 mm diameter. A PCB is attached to one of the flat sides of the cylinder, including the basic circuitry for rectification filtering and energy storage. There is enough room at both flat sides of the device to include additional circuitry in a compact manner.

In addition to physical reasons, dimensions and weight of the device are very practical in terms of manipulation, transport and installation. It may also contain, as shown before, the required electronics not only for the power conversion, but also for sensing, processing and communication as it is required to analyze vibrations for condition monitoring purposes. A larger device would obviously produce more energy, however at the expense of usability.

In the next section we will describe a comprehensive model for the device, and show its possibilities and practical limits.

3. Device model and theoretical limitations

The physical characteristics of the harvesting device have been described in the previous section. A detailed model of the system is described hereafter considering both its mechanical and electromagnetic configuration. The model will be general enough to optimize the system for different operating conditions and flexible enough to allow the analysis of other similar configurations (e.g. different number of masses).

Referring from now on to Fig. 6 for the parameters definitions to obtain dynamic equations, it will be assumed that the device moves under arbitrary displacements in the x and y directions $x(t)$ and $y(t)$. Under this excitation, the ith (center of) mass suffers the following displacement with respect to the inertial frame of reference. Their derivatives represent the velocity of the center of mass.

$$x_i(t) = x(t) + L_G\, cos(\theta_i(t)\,) \tag{1}$$

$$y_i(t) = y(t) + L_G sin(\theta_i(t)\,) \tag{2}$$

$$with\ \ i = 1, 2, 3$$

The dynamic equations can be obtained by resorting to the Euler-Lagrange formulation where we need to obtain first the kinetic and magnetic energy contributions, which constitute the conservative part. Regarding the kinetic energy, it can be expressed for the ith mass as.

$$E_{ki} = \frac{1}{2} m v_i^2 + \frac{1}{2} I_{zz} \dot{\theta}_i^{\,2} \tag{3}$$

Where I_{ZZ} is the moment of inertia with respect to the center of gravity of the moving mass. Taking into account that

$$v_i^2 = \dot{x}_i^{\,2} + \dot{y}_i^{\,2} \tag{4}$$

the kinetic energy can be expressed as:

$$E_{ki}(t) = \sum_{i=1}^{3} \frac{1}{2} I_{zz} \dot{\theta}_i^{\,2} + \frac{1}{2} m \left\{ \dot{x}^2 + \dot{y}^2 + L_G \dot{\theta}_i^{\,2} + 2 L_G \dot{\theta}_i \left(\cos(\theta_i) \dot{y} - sin(\theta_i) \dot{x} \right) \right\} \tag{5}$$

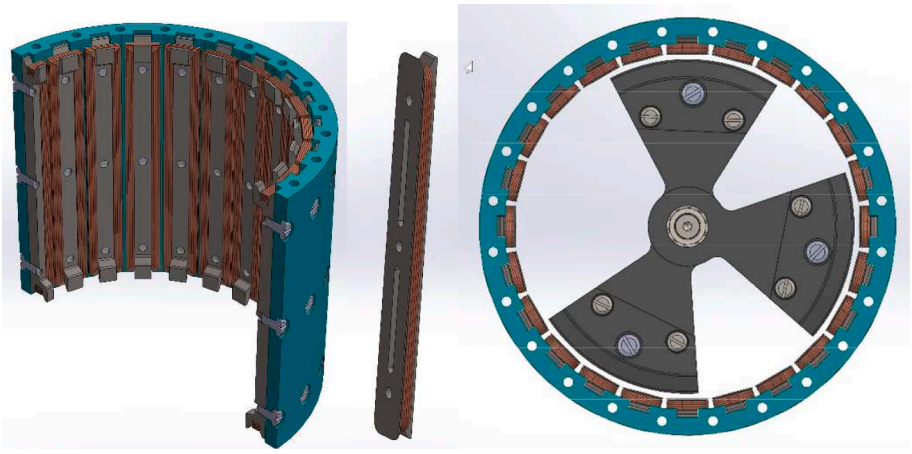

Fig. 5. (a) Half case with coils, (b) Single coil, and (c) Upper view with three masses and casing.

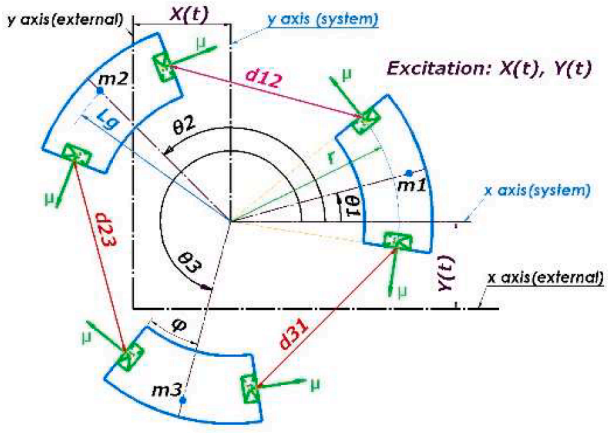

Fig. 6. Coordinate system and variables for the model.

The magnetic energy due to the interaction between the magnets plays the role of the elastic energy of a conventional resonator, but has in this case a strong nonlinear behavior. We will assume only the magnetic interaction between adjacent magnets at the extremes of the moving masses, which is the responsible for the repulsion between masses when they get closer. The total magnetic energy is, according to a dipole model [35], expressed in equation (6) where μ is the magnetic moment of the magnets and d_{ij} their instantaneous distances.

$$E_P(t) = \frac{\mu^2}{4r^2}\left[\frac{8r^2 - d_{12}^2}{d_{12}^3} + \frac{8r^2 - d_{23}^2}{d_{23}^3} + \frac{8r^2 - d_{31}^2}{d_{31}^3}\right] \tag{6}$$

where

$$d_{ij}(t) = \sqrt{2}r\sqrt{1 - cos(2\varphi + \theta_i - \theta_j)} \tag{7}$$

The masses are also subjected to the damping produced by the interaction between magnets and coils connected to an electrical impedance. This is actually the energy extraction (transduction) mechanism which has to be optimized to harvest as much energy as possible. The instantaneous power extracted can be assumed to be proportional to the angular velocity [15], and can be written as:

$$P = \frac{dE}{dt} = br^2\sum_{i=1}^{3}\dot{\theta}_i^{\,2} \tag{8}$$

where b is the damping coefficient, which will depend on the interaction between coils and magnets. The average power is obviously calculated by integrating the instantaneous power over time and dividing by the time interval. The above expression will serve to estimate the upper limit of the power that can be extracted from the harvester.

The Lagrangian for the conservative system is:

$$L = E_k - E_p \tag{9}$$

where E_k accounts for the kinetic energy of the three masses. The dissipative contribution can be introduced into the Lagrangian formulation through the Rayleigh dissipation function obtained as [36]:

$$E_D = \frac{1}{2}\frac{dE}{dt} \tag{10}$$

Then, the three dynamic differential equations for the system can be obtained as:

$$\frac{d}{dt}\left(\frac{\partial L}{\partial \dot{\theta}_i}\right) - \frac{\partial L}{\partial \theta_i} + \frac{\partial E_D}{\partial \dot{\theta}_i} = 0 \tag{11}$$

which produces three coupled equations, which can be expressed in a compact form as follows:

$$\begin{aligned}
&\ddot{\theta}_1\left(mL_G^2 + I_{zz}\right) + br^2\dot{\theta}_1 + \frac{\mu^2(\gamma_2 - \gamma_3 + \delta_2 - \delta_3)}{4r^2} + mL_G(cos(\theta_1)\ddot{y} - sin(\theta_1)\ddot{x}) = 0\\
&\ddot{\theta}_2\left(mL_G^2 + I_{zz}\right) + br^2\dot{\theta}_2 + \frac{\mu^2(\gamma_3 - \gamma_1 + \delta_3 - \delta_1)}{4r^2} + mL_G(cos(\theta_2)\ddot{y} - sin(\theta_2)\ddot{x}) = 0\\
&\ddot{\theta}_3\left(mL_G^2 + I_{zz}\right) + br^2\dot{\theta}_3 + \frac{\mu^2(\gamma_1 - \gamma_2 + \delta_1 - \delta_2)}{4r^2} + mL_G(cos(\theta_3)\ddot{y} - sin(\theta_3)\ddot{x}) = 0
\end{aligned} \tag{12}$$

where σ_1, σ_2 and σ_3 depend on the angular displacements as follows:

$$\begin{aligned}
\sigma_1 &= 2\varphi + \theta_2 - \theta_3\\
\sigma_2 &= 2\varphi + \theta_3 - \theta_1\\
\sigma_3 &= 2\varphi + \theta_1 - \theta_2
\end{aligned} \tag{13}$$

And constants γ_i, δ_i are defined as follows.

$$\gamma_i = \frac{\sqrt{2}r^2\sin\sigma_i}{2\,r^3\,(1 - \cos\sigma_i)^{5/2}} \qquad \delta_i = \frac{3\gamma_i\,(\cos\sigma_i + 3)}{2\,(1 - \cos\sigma_i)} \tag{14}$$

The above equations are strongly non-linear in the variables θ_i and

cannot be analytically solved. Therefore, closed form expressions for displacements and velocities, even in the case of harmonic excitation, are not available. The system can be seen as a complex spring/damper mechanism, Fig. 1(c), where stiffness is a strongly nonlinear function of the distance, i.e. angular separation, of masses. Such stiffness is produced by the magnetic repulsion between blades which results from the residual magnetic field at their edges. Fig. 7 shows the potential energy of the system resulting from only the lateral magnets interaction of the three masses, which is the most significant. The total magnetic energy is also plotted.

To calculate the curves, we have assumed one mass is locked, while the other two are symmetrically placed with respect to the first one. Their range of movement goes from 60° to 150°, which is the maximum displacement taking into account masses dimensions. Fig. 8 shows the two extreme and one intermediate (i.e. equilibrium) positions respectively. To properly understand Fig. 7, note that Ep12 and Ep13 are "symmetrical" with respect to 120°, but the right part (from 120° to 150°) is a compressed version of the left part by a factor of 2. This is due to the fact that masses 2 and 3 move symmetrically while mass 1 is locked. It is evident from the curves that potential energy is far from exhibiting a quadratic behavior as would be the case of a typical spring with a restoring force linearly dependent on elongation.

For our purposes it will suffice for the moment a numerical solution to estimate the dynamics (displacement, velocities) of the masses and the energy which potentially may be extracted under predicted working conditions. The comparison of simulations against practical measurements will allow validating the model and tuning some physical parameters such as magnetic moment or damping, which are not accurately known. Moreover, damping depends on the electrical load and thus must be estimated for every condition. The procedure for assessing the validity of the model and to estimate such parameters will be presented in the next section.

4. Model parameters estimation and experimental Setup.

The harvester model built in the previous section has some parameters whose values are not easy to know a priori. The parameters of mass (m), center of gravity position (L_G), radius (r), second moment of inertia (I_{zz}) and angle φ can be determined with sufficient accuracy using CAD software. However, it is much more complicated to give a realistic and precise value for the parameters μ and b as they are related to a very complex magnetic field, as shown in Fig. 4.

In order to determine values of μ and b for the actual harvester, an experiment and a subsequent parameter estimation process have been designed. Fortunately, the dynamic equations can be written linearly with respect to the parameters b and $\mu' = \mu^2$ so that the estimation can be carried out with a simple linear regression from experimental data.

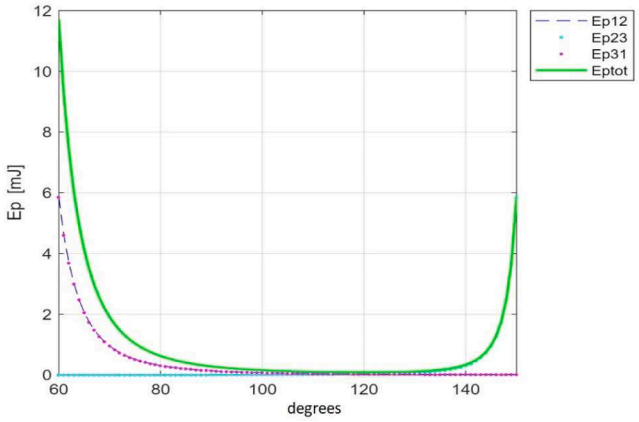

Fig. 7. Potential Energy.

Let us rewrite Eq. (12) in a compact manner as:

$$\mathbf{K}_\mu \mu' + \mathbf{K}_b b = \begin{bmatrix}\mathbf{K}_\mu \mathbf{K}_b\end{bmatrix} \begin{Bmatrix} \mu' \\ b \end{Bmatrix} = \mathbf{K}\mathbf{p} = \tau \tag{15}$$

Where τ is the sum of two vectors, namely, the external excitation that depends on $\ddot{x}$ and $\ddot{y}$ and the inertia terms. Terms $\mathbf{K}_\mu$ and $\mathbf{K}_b$ are 3x1 vectors that multiply to μ' and b, respectively, in Eq.(15). As this equation is valid for any time instant, we can write it for n instants obtaining an overdetermined system of equations:

$$\chi = \begin{Bmatrix} \tau_1 \\ \vdots \\ \tau_n \end{Bmatrix} = \begin{bmatrix} \mathbf{K}_1 \\ \vdots \\ \mathbf{K}_n \end{bmatrix} \mathbf{p} = \mathbf{W}\mathbf{p} \tag{16}$$

Solving this linear system of equations by, for instance, least squares yields an estimate for $\mathbf{p}$:

$$\hat{\mathbf{p}} = \left(\mathbf{W}^{\mathrm{T}}\mathbf{W}\right)^{-1}\mathbf{W}^{\mathrm{T}}\chi \tag{17}$$

In order to apply this algorithm to estimate vector $\mathbf{p}$, it still remains to evaluate $\mathbf{W}$ and τ with the measured values of θ_1, θ_2 and θ_3 and their first and second derivatives. It is not easy to measure the angular displacement of every mass relative to the casing, and to do it, we have resorted to an image based experimental setup, shown in Fig. 9.

The harvester is excited by a shaker which generates sinusoidal oscillations in a range from 0.2 to 1.2 Hz with variable amplitudes up to ± 50 mm. A video camera, actually a mobile phone in slow motion mode, is attached to the moving platform where the harvester is fixed. The camera focuses the upper side of the harvester (with a transparent cover), capturing 240 frames per second. Colored circles are stuck over each one of the masses as shown in Fig. 9 and also in Fig. 10(a). An application is developed making use of the Artificial Vision Toolbox of Matlab, which determines the center of each circle, and follows their movement when the harvester is excited. Then, from the moving coordinates measured, a simple geometric postprocessing has been developed to calculate the instantaneous rotation angle of each mass with respect to the horizontal axis, as shown in Fig. 10(b).

Simultaneously, the voltages at the 24 coils can be also measured and transferred to the PC for post processing, power calculation, and storage. Different loads can be easily connected to measure the power generated under different conditions. The harvester also incorporates an accelerometer (ADXL345) to simultaneously measure actual accelerations. All this circuitry is compacted on a PCB connected to the lower side of the harvester, partially seen in Fig. 9. Image measurements are synchronized to electrical measurements by a led indicator as the trigger condition.

To obtain data sequences to solve the identification problem, it was decided to measure the transient resulting from the symmetrical displacement of two masses (green and red) from the equilibrium position at ± 60°, leaving the third one (blue) locked at $\theta_1 = 0°$, in such a way that $\ddot{x} = \ddot{y} = 0$ at all times. By releasing the masses under these initial conditions, we obtained the time series for the angles.

Once the instantaneous values of the angles have been measured, the values for their derivatives need to be calculated, to be introduced into the equations. As the algorithm used for estimating the angles is based on relatively noisy measures of the markers' positions, it is not suitable to apply direct numerical differentiation methods to obtain both the velocities and accelerations. In contrast, the Total Variation smoothing algorithm [37–39] has been applied to obtain reliable first and second derivatives. The results for angles and angular velocity and acceleration are shown in Fig. 11.

By evaluating $\mathbf{W}$ and τ with the values obtained above and solving for Eq. (17), the following values have been obtained for $\hat{\mathbf{p}}$, namely $\hat{\mu} = 140 \bullet 10^{-6} J/T$ and $\hat{b} = 160 \bullet 10^{-3} kg/s$. The measured and estimated values of τ are represented in Fig. 12, showing a very good fit between measured and estimated values. We note that these values have been obtained when the harvester is not charged and thus damping can be

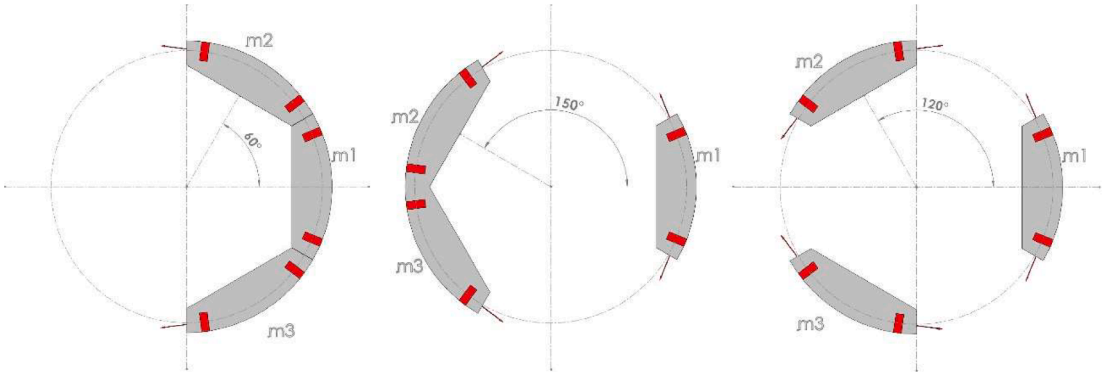

Fig. 8. Movement of the masses to calculate the magnetic energy: extreme and intermediate (equilibrium) position.

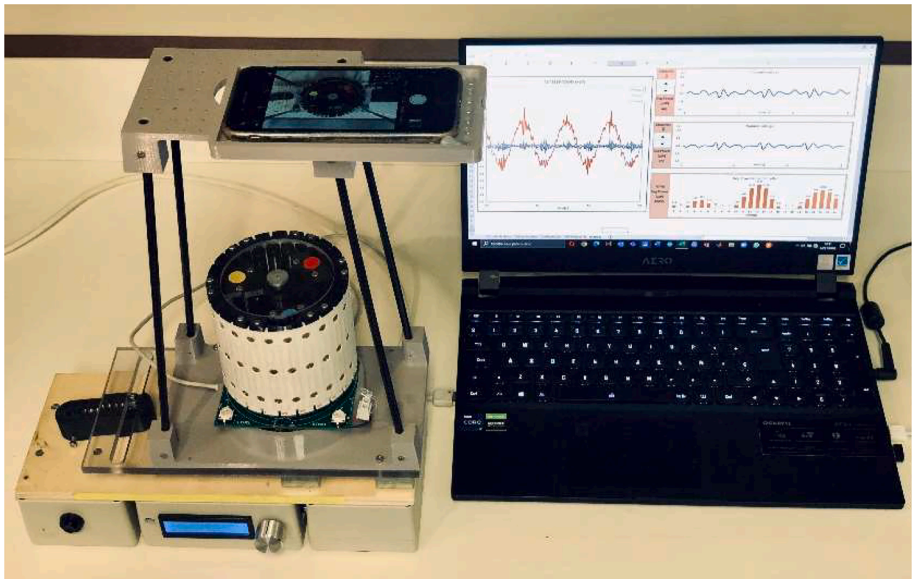

Fig. 9. Experimental setup. Harvester on the shaker with a zenithal video camera (mobile phone), which moves attached to the harvester.

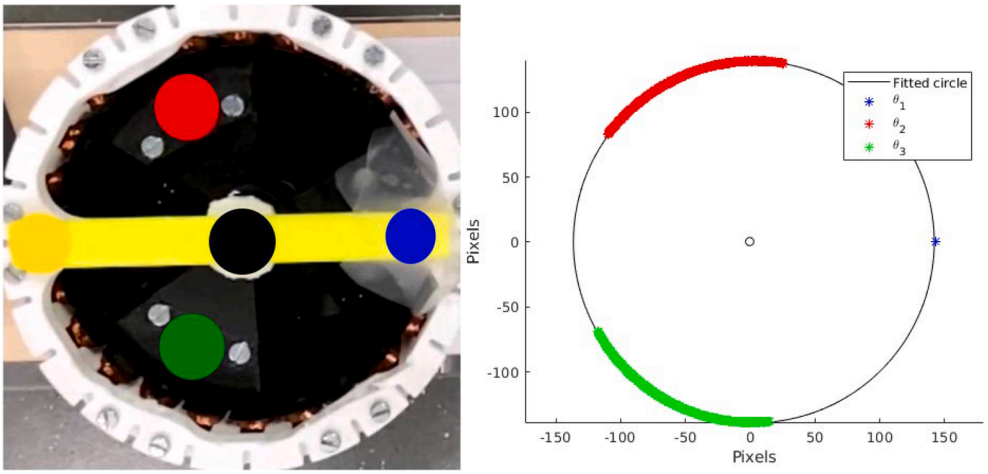

Fig. 10. (a) upper view of the harvester with colored stickers on the masses to measure their movement. (b) Postprocessing: extrapolation to positions on a perfect circle.

associated to the internal friction.

5. Simulations and experimental Results.

Once we have validated our model and estimated its relevant parameters, we are in the position to analyze the behavior of our system

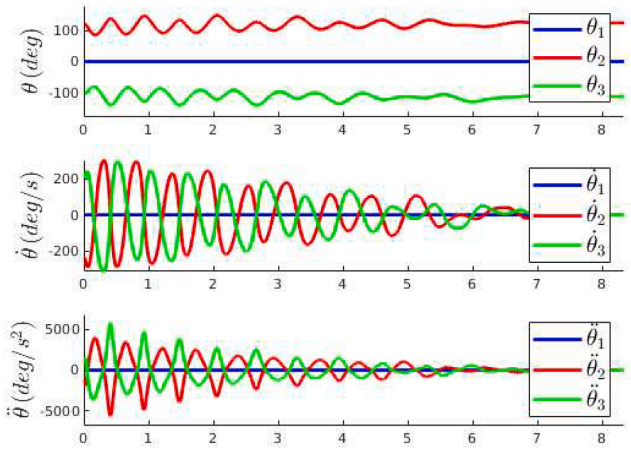

Fig. 11. Measured angles for the three masses with their first and second derivatives (mass 1 fixed). Time axis is in seconds.

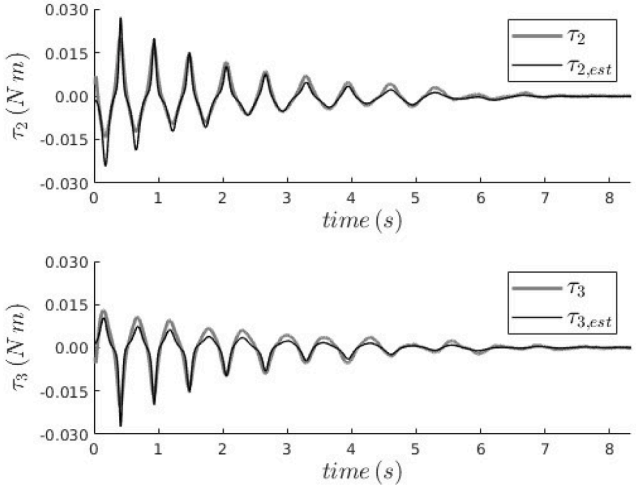

Fig. 12. Measured and estimated values for τ.

under any excitation condition. We are interested first in estimating the natural frequency of the device, which can be deduced from its transient behavior. The homogeneous response of the differential equations, when initial conditions for two masses are different from the repose ones, is shown in Fig. 13. This corresponds to the symmetrical movement of two masses, while the third one is locked.

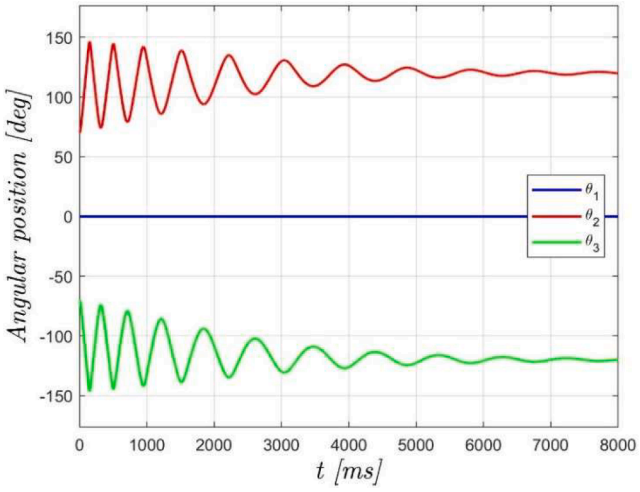

Fig. 13. Simulated transient response of one of the masses when separated from its equilibrium position.

The response is not a typical exponentially decaying sinusoid, as would be the case of a linear system. Actually, our system could be interpreted in terms of a "nonlinear" stiffness resulting from the magnetic potential energy, which is represented in Fig. 7. The underlying oscillation frequency obtained from Fig. 13 decays from values up to 4 Hz, depending on the initial displacement, to approximately 1 Hz when the angle excursions are very low.

The above results could lead to an estimation of the resonance frequency of the device, though the concept does not rigorously apply to nonlinear systems such as this. Actually, the oscillation frequency varies as amplitude diminishes, which agrees with the observation that the equivalent stiffness grows with amplitude. The resonance frequency has also been estimated for small angular deviations from the equilibrium position by linearizing the potential energy equation, assuming a constant stiffness and thus a quadratic dependence of the energy on θ_i. By using the Rayleigh method to calculate the natural frequency, the resulting value is 1.05 Hz, which is in very good agreement with observations.

Such natural oscillation, regardless of the angle variations, is above the intended range of operation and cannot be exploited to optimize the harvested energy. This property is common to mechanical harvesters that purport to operate at such low frequencies, as shown for instance in [40].

We can also simulate the behavior of our harvester under stationary conditions. The dynamical equations have been numerically solved for a sinusoidal excitation, i.e.

$x(t) = A\cos(2\pi ft) y(t) = 0$ (12)for different amplitudes and frequencies in the ranges from$A = 20$ to 50 mm and$f = 0.3$ to 1.2 Hz which are within the specifications of the application at hand. The fact that the movement in one of the axes, $y(t)$, has been assumed null is not a limitation since the masses have been arbitrarily located out of the equilibrium position, with neither of them aligned with the direction of the movement. Fig. 14(a) to 14(f) show the angular displacement of the three masses for several representative excitation amplitudes and frequencies. The displacements are referenced to the equilibrium position of each blade. The system orientates in such a way that excursion is wider in one of the blades while the others move similarly in a lower extent.

Another observation is that when internal displacements are small, their shape is almost sinusoidal, whereas for large displacements signal is distorted. This is obviously a consequence of the non-constant stiffness due to the magnetic field. Moreover, movements in opposite directions are not coincident, due to the lack of symmetry in the position of the masses, as also reflects potential energy depicted in Fig. 7.

What is relevant here is to see to which extent the model is able to estimate the upper bounds of the energy that can be extracted from the device here proposed. To this end, we have first measured the power generated by the harvester by measuring and adding the power generated by all 24 coils, when each one of them is loaded by a resistor equal to the coil resistance, around 100 Ω. These are ideal conditions in the sense that power extracted is the maximum achievable, and there is no further power conversion circuitry to obtain a DC voltage which may introduce losses. From this information, power can be calculated for different loads.

The measurements have been carried out with the setup described in previous section, for four different excitation frequencies: 0.3, 0.6, 0.9 and 1.2 Hz, the same used in the simulations, and 50 mm excursions. It is illustrative to show first the voltage waveforms generated at the coil's outputs under such sinusoidal excitations. In Fig. 15 we show three coils voltages measured at frequencies of 0.6 and 0.9 Hz. The three waveforms correspond to the three coils (out of the 24) that in the represented time frame produce the maximum average power, since they are the closest to the masses position.

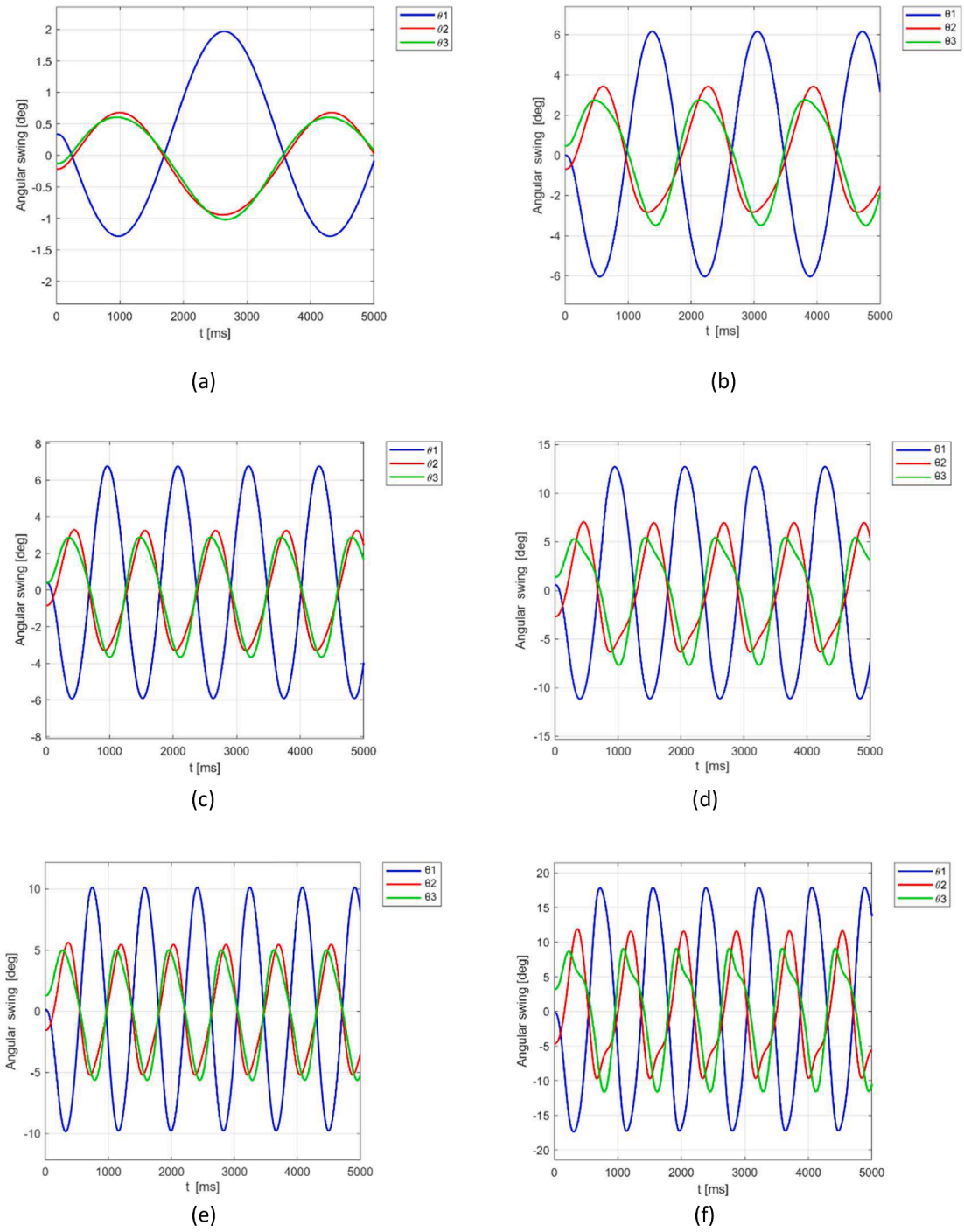

Fig. 14. Movement of the three blades at the following conditions (a) 50 mm at 0.3 Hz, (b) 50 mm at 0.6 Hz, (c) 25 mm at 0.9 Hz, (d) 50 mm at 0.9 Hz, (e) 25 mm at 1 Hz, (f) 50 mm at 1.2 Hz

The differences between cases a) and b) are evident. First, voltage levels at 0.9 Hz (voltage units 1 V) are higher than those at 0.6 Hz (voltage units 0.5 V), due to the larger excursion of the masses. As predicted, small increments in the frequency produce notable changes in voltages and thus in the power generated. Second, waveform for 0.9 Hz contains higher frequencies since, apart from the limited increase in the excitation frequency, masses move in a wider range with respect to the coil. Since the magnetic field generated by each mass is not uniform, see Fig. 4, such variations induce variations in the coil voltage which become evident at higher excitation frequencies.

Power distributes among the coils in an unpredictable way, depending on the excitation direction and the coils position. In Fig. 16 we show an example when one of the masses is almost still and the other two move with similar excursions.

By summing up the power generated by all coils, the results are 10 μw, 327 μw, 3.0 mW and 9.3 mW for frequencies of 0.3, 0.6, 0.9 and 1.2 Hz respectively. We recall that such measurements correspond to the optimum power transfer when load matches output impedance of the coils. If a simplified rectifying circuit is added, the measured values drop to 85 μw, 1.7 mW and 5.5 mW for frequencies of 0.6, 0.9 and 1.2 Hz respectively. To get those values, voltages at the coils outputs have been rectified and applied to a high valued capacitor. Power is calculated as the ratio of energy (charge) stored in a given time. These values are, as expected, lower than those obtained without any power converting

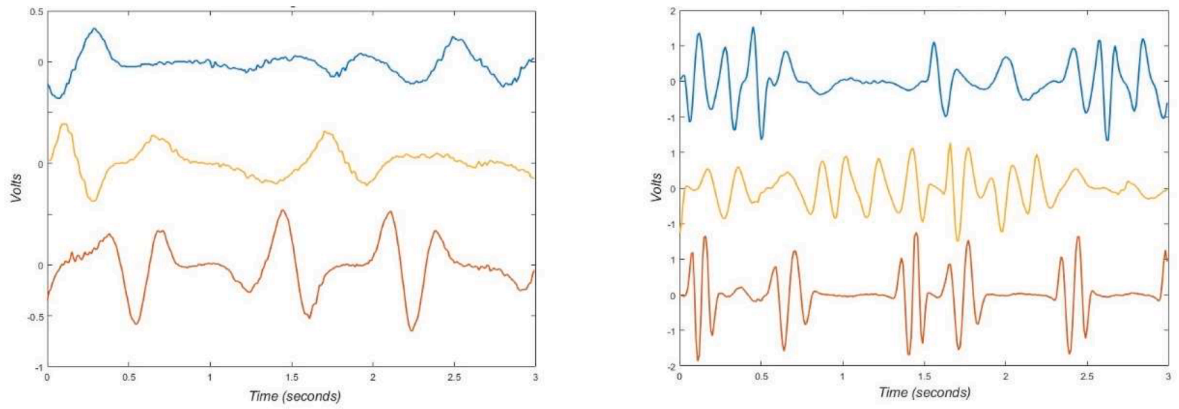

Fig. 15. Coil voltages measured at (a) 0.6 Hz and (b) 0.9 Hz.

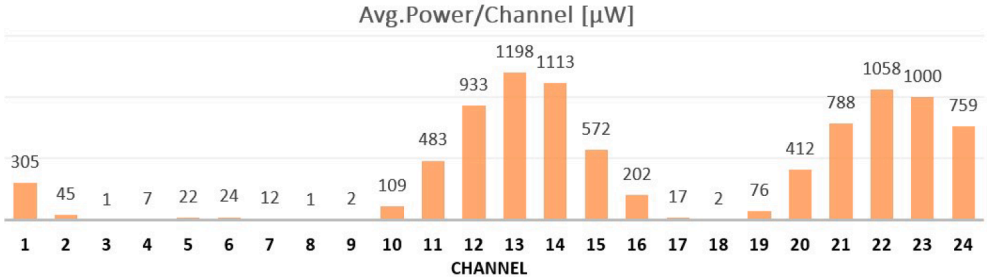

Fig. 16. Average Power measured in μw on each one of the coils.

circuitry.

Table 1 summarizes these measured results (columns 4 and 5), and compares them with the values calculated from the model, column 3, according to expression (8), by integrating it over time and dividing by the time interval. They are calculated under optimum conditions, i.e, the highest mechanical power generation. Discrepancies between measurements and simulations are relatively higher at the lowest frequencies, but, in any case, can be mainly attributed to the internal friction of the bearings and of course to the EM conversion (parasitic impedances). It is noteworthy, as anticipated, how generated power strongly depends on the frequency for both simulated and measured values. The influence of the displacement values is less relevant. This is graphically shown in Fig. 17 where calculated power is plotted against frequency and amplitude.

Simulated power values follow approximately a cubic dependence on the excitation frequency, which agrees with the results obtained in [30]. On the contrary, the measured energy ratios for constant frequency variations do not seem to obey a defined pattern, and the dependence on frequency is of higher order than three. The disparity can be attributed to the fact that in the mentioned reference, and in our simulations, what it is actually calculated is an upper bound of the mechanical energy. The transduction mechanism is not able to extract all of the available mechanical energy due to the reasons mentioned above. By considering the high order dependence on frequency, the need to properly dimension the device for the desired frequency range is of utmost importance.

Table 1
Harvested Avg. power in μW, calculated and measured.

EXCITATION		Calculated Average Power	Measured Average Power (all coils)	Measured Average Power (with rectifying)
[mm]	[Hz]			
50.0	0.3	3.340	10	0
50.0	0.6	6.122	327	84.8
50.0	0.9	18.763	3.039	1.726
50.0	1.2	44.699	9.272	5.527

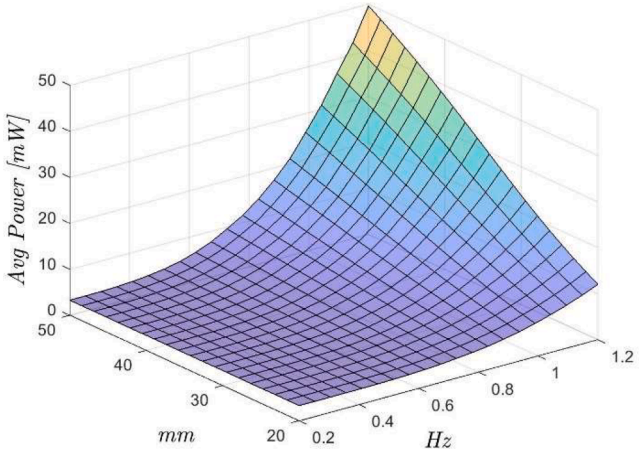

Fig. 17. Average power as a function of displacement and frequency.

Regarding the disparities between the two measured power values, they are due to the use in the worst case of a very simple rectifying circuit. As we said before, coils outputs have been rectified and applied to a high valued capacitor. This rectifying circuit stores the charge coming from only the coil exhibiting the highest voltage at a given instant, spoiling a relevant portion of the power available in other coils. Moreover, the threshold voltage of diodes precludes charging the capacitor when voltages are very low, and thus reduce dramatically the extracted power at low frequencies. A more elaborated circuitry will allow higher efficiency in the power conversion.

Above simulations correspond to ideal harmonic excitation which give information of how the system works depending on the frequency and amplitude. The behavior is, as we have shown, highly nonlinear and therefore cannot be characterized by either impulse responses or

transfer functions. However, the device is intended for an application, vibration in wind turbines, where the excitation is broadband with a power not uniformly distributed in frequency. Therefore, it is not straightforward from simulations under harmonic excitation to estimate the power which can be expected in the application at hand. An experimental test in real conditions will be programmed in the next months but for the moment, making use of our model, we can make simulations with real acceleration signals measured on top of wind turbines.

We have available accelerations measured at the nacelle of a wind tower in both x and y axis, on a plane parallel to ground. The wind turbine corresponds to a 3 MW machine with a first Fore-Aft (1FA) mode around 0.38 Hz and a 3P frequency around 0.65 Hz. Second FA mode is located at 1.7 Hz. This means that vibration power is mostly concentrated between 0.2 Hz and 2 Hz. Peak acceleration values are around 0.04 g, with RMS values around 0.008 g resulting from the operation in the nominal power regime. A representative example is shown in Fig. 18 where the upper waveforms represent the measured accelerations both x and y axis. The estimated instantaneous power calculated with our model is shown in the lower graph. The power generation peaks reach up to 4 mW although the average power generated is around 400 μW.

6. Comparison with State-of-the-Art harvesters

It is not easy to assess how the proposed harvester compares with other solutions intended for ultra-low frequencies. As mentioned above, there are only three references reporting devices working a little lower than 1 Hz, and even in those cases, the application is different. The multidirectional operation is another characteristic of our device which is not found in most harversters that obtain energy from vibration. To make things even more complicated, there is not a widely accepted figure of merit which may serve to compare harvesters working at different frequency ranges, not to say different working principles.

However, we will try to make a fair comparison with other state of the art disclosed harversters. First, in Table 2 we summarize a comparison of the three mentioned devices with our harvester, including their most relevant parameters. We have also included in the table the device described in reference [26], because, although it works at higher frequencies, it describes a multidirectional harvester. The data in Table 2 have been extracted from the original papers to which reference is made. In the last columns of Table 2 we include the calculation of two

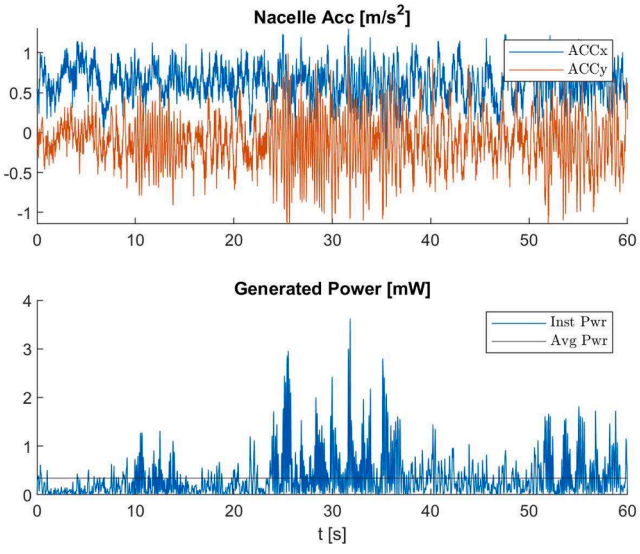

Fig. 18. Accelerations measured in the two axis and Instantaneous power generated for a wind turbine. (DC level for ACCx has been shifted to clearly distinguish it from ACCy).

alternative figures of merit. The first one is the most widely used, though not necessarily accepted, which normalizes power (Normalized Power Density-NPD) with respect to frequency, squared acceleration and volume. We also propose another figure of merit which normalizes with respect to frequency, acceleration and volume raised to 4/3, since the product of these three parameters is proportional, according to [30], to the maximum achievable mechanical energy. With this table, readers may easily draw their own conclusions. In the next paragraphs we will highlight our own conclusions.

Reference [23] describes a device giving 60 μW at 0.8 Hz for an acceleration 0.06 g. Our device gives experimentally 327 μW, a fivefold increase, at similar accelerations but at lower frequency (0.6 Hz). We could say that our device generates much more energy under similar conditions, but to be honest, this is achieved with a bulkier device (3.6 times). If we compare the two figures of merit, the values are comparable for both devices at similar frequencies meaning that the two harversters have similar efficiencies. However, our device is multidirectional, which is not the case of the device in [23] that is not oriented to any specific application. Human movement, and even wind towers, are mentioned as target applications, but the lack of multidirectionality limits the possible use in wind towers to the nacelle.

In reference [28], 1.6mW are reported at 0.9 Hz and 0.23 g, versus our 3 mW at exactly the same frequency and lower accelerations, 0.16 g. Their device has much larger dimensions, resulting in figures of merit clearly favorable to our device. The proposed device is in this case multidirectional, but intended to extract energy from ocean waves. The internal mechanism combines frequency up-conversion and piezoelectric transduction, what explains its much lower efficiency. Anyway, this device is the closest to ours in terms of operation bandwidth.

In reference [10] the authors report 3.77 mW average power for a human-induced motion frequency range between 0.9 and 1.93 Hz, and 0.12 g excitation. This is a “broadband” excitation which takes advantage of the higher efficiency at high frequencies. In our case, we can achieve values 9 mW with only 0.3 g and a frequency of 1.2 Hz. Our results are, in absolute terms, better, considering that they correspond to a pure harmonic excitation. The device, very imaginative, is based on piezoelectric transduction and can capture energy in every direction. It is however bulky and heavy, resulting in very poor figures of merit well below the figures we achieve.

Regarding reference [26], which we included because it is a multidirectional harvester, it reports 9.8 μW at 2.6 Hz and 0.03 g. Being comparable in size to our harvester, it is evident that ours is much more efficient (e.g. 327 μW at 0.6 Hz and 0.07 g).

To have another benchmarking with devices working at higher frequencies, up to 10 Hz, unidirectional in all cases, we also include Table 3 with the most relevant parameters of the devices reported working in those conditions. From it, the reader can draw his/her own conclusions. Direct comparisons are not possible, since not only the frequency range is different (higher) but also acceleration levels are in general higher than those found in our application. However, we will try to make some comparisons of our harvester at least versus those closest in frequency. To this end, we have carried out some experimental tests beyond the limits originally intended for our harvester. This means that the excursions suffered by the masses exceed the available range, producing impacts between them with a saturation in the power produced.

In reference [24], a device giving 8.37 mW at 2 Hz with accelerations of 0.1 g is demonstrated. The device proposed here generates 10 mW at the same frequency, and at 0.16 g. The power numbers are very similar, though our harvester is bulkier but operating at conditions which are as we said, not optimum. It is however surprising to us how in this last device, average power generated does not significantly change with frequency.

Reference [11] describes a triboelectric device which is able to generate 14.7 mW at 2.25 Hz and accelerations of 4.07 g. We could not test our device at such high accelerations, but at just 1 g, and the same frequency we obtained 47 mW. The device in [11] is larger than the

Table 2
Comparison with the closest published harvesters.

Ref.	Power [μW]	Excitation Type		Gen. Principle			Volume [cm^3]	Amplitud [mm]	Freq. [Hz]	Accel. [g]	$\frac{\mu W}{cm^3 g^2 Hz}$	$\frac{\mu W}{cm^4 g Hz}$
				EM	PE	TEN						
[23]	60	Hor.	1D	X			192,0	N/A	0,80	0,06	**104,21**	**1,11**
[28]	1.600,0	Hor.	2D		X		4.704,0	70,0	0,90	0,23	**7,26**	**0,10**
[10]	3,8	Hor.	2D		X		1.156,0	N/A	0,89	0,12	**0,25**	**0,003**
[26]	9,8	Hor.	2D		X		471,0	N/A	2,60	0,03	**8,89**	**0,03**
This work	327,0	Hor	2D	X			706,9	50,0	0,6	0,07	**38,1**	**1,19**
	3.039,0							50,0	0,9	0,16	**102,2**	**3,39**
	9.272,0							50,0	1,2	0,29	**77,6**	**4,21**

Legend: EM = Electromagnetic, PE = Piezoelectric, TEN = Triboelectric, Hor = Horizontal, Ver = Vertical, 1D = Unidirectional, 2D = Multidirectional.

Table 3
Comparison of published harvesters up to 10 Hz.

Ref.	Power [mW]	Excitation Type		Gen. Principle			Volume [cm^3]	Amplitud [mm]	Freq. [Hz]	Accel. [g]	$\frac{\mu W}{cm^3 g^2 Hz}$	$\frac{\mu W}{cm^4 g Hz}$
				EM	PE	TEN						
[12]	2.0	Hor.	1D	X			65,8	6,0	3,5	0,30	**99,3**	**7,26**
[17]	85.8	H/V	1D	X	X	X	23,2	N/A	3,0	1,00	**1.233,6**	**432,53**
[21]	1.9	Vert.	1D	X			5,9	N/A	5,17	2,06	**15,2**	**17,32**
[18]	11.7	H/V	1D	X		X	30,9	N/A	5,0	0,50	**304,3**	**48,50**
[41]	0.71	Vert.	1D	X			1,6	N/A	10,0	0,52	**165,5**	**73,58**
[20]	0.039	Vert.	1D	X			3,7	N/A	10,0	1,00	**352,9**	**0,69**
[11]	14.7	Vert.	1D			X	1.254,9	200,0	2,25	4,07	**0,3**	**0,12**
[27]	23.5	Hor.	1D	X			31,4	40,0	4,5	3,26	**15,6**	**16,16**
[19]	330.0	Vert.	1D	X	X		100,0	N/A	7,0	0,70	**962,1**	**145,09**
[24]	8.4	Hor.	1D	X			153,9	N/A	2,0	0,10	**2.718,6**	**50,73**

Legend: EM = Electromagnetic, PE=Piezoelectric, TEN=Triboelectric, Hor=Horizontal, Ver=Vertical, 1D=Unidirectional.

ours, and therefore we get a much higher efficiency, apart from the multidirectional operation. We recall that harvester in [11] is based on the triboelectric effect for energy conversion that in general is less efficient in terms of power generation than the electromagnetic conversion we use.

Going a bit higher in frequency, we find reference [17] where authors report remarkable power peaks of 85.8 mW at 3 Hz for 1 g accelerations. This is a peak value produced by a device comprising several mechanisms of energy harvesting, though the EM section would account for less than half of the total power. We have tested our device, at its very limit, under the same conditions, 3 Hz @ 1 g, obtaining average (not peak), powers of 78 mW which would be even higher if the masses did not collide with each other. Again, though our numbers are better, they get their results with a much smaller device.

Last, we would like to mention harvester described in [12], intended to scavenge energy from the human movement and also unidirectional in nature. Data reported correspond to 3.5 Hz and accelerations of 0.3 g, giving a power of 2 mW. We have measured 38,5 mW at 3.0 Hz and 0.5 g that considering the different sizes, and the resulting NPD, can be seen as similar in terms of efficiency.

PE = Piezoelectric, TEN = Triboelectric, Hor = Horizontal, Ver = Vertical, 1D = Unidirectional,

As a conclusion of the previous analysis, we can say that our device exhibits better efficiency than those harvesters that work in the same frequency range. Such conclusion is based on the direct comparison of the generated power under similar working conditions (Table 2), and on the NPD values. Regarding harvesters working at higher frequencies (Table 3), always below 10 Hz, direct comparisons are not easy. So, we have tried to make a fair comparison with at least those closer in frequency. To this end we have carried out some measurements with our device working beyond the limits set by the original specifications. Considering such a circumstance, our harvester remains very competitive.

The comparison has served us to confirm that our device, whose intended application is very different from those reported so far, is within the state of the art of akin harvesters and is well suited for the application.

As a final note in this section, we would like to express our conclusion regarding the limited value of the Normalized Power Densities as figures of merit to characterize in a single number the efficiency of a harvester, particularly when we try to compare harvesters based on different transduction principles and working in different ranges of operation. Our own harvester, see Table 2, gives very distinct numbers at different working conditions. This is mainly due to the effects of the load, and second order effects as well (i.e. friction) whose influence is very different depending on the operating conditions.

7. Conclusions

We have demonstrated the practical feasibility of a novel device which can harvest energy from oscillating movements on a plane in the range of 1 Hz and below. A prototype has been designed, built and experimentally tested, and a numerical model developed to theoretically support our findings. The target application is wind turbines, where autonomous sensor networks need to be deployed at the tower or nacelle to measure accelerations for SHM purposes. The device fills the need for harvesters that can work in the aforementioned conditions of ultra-low frequencies, motion ranges, and multiple directions. The harvester can potentially provide the energy required by low-power devices, or at least extend considerably the lifetime of batteries. Though references for benchmarking are scarce, we believe the device proposed is very efficient in terms of energy scavenging, with still room for improvement.

Efficiency comparisons have been made with some of the devices in the literature that are designed to operate in conditions relatively similar to those of wind turbines. By direct comparisons, and according to the figures of merit used in the literature, these comparisons show that the device designed in this paper has very good power generation levels.

The lessons learnt with this prototype have paved the way to improvements and new ideas which may potentially increase significantly the harvested energy. One evident enhancement is the increase of mass making use of metallic non-magnetic materials. The use of four masses instead of three shows, according to simulations, a significant increase in

energy due to a more optimum placement of the masses with respect to the movement direction. A redesign of the coils, to reduce their number and their parasitic impedance, would be also positive, along with a more elaborated design of the rectifying and charging circuitry. It is also important to reduce to a minimum all sources of internal friction. Apart from this, other ideas are in progress and will be developed.

Declaration of Competing Interest

The authors declare the following financial interests/personal relationships which may be considered as potential competing interests: Alfonso Carlosena reports financial support was provided by Spanish Research Agency. Xabier Iriarte reports financial support was provided by Navarra Government General Directorate of Industry Energy and Strategic Projects S3.

Data availability

Data will be made available on request.

Acknowledgements

This work has been supported by the Spanish Research Agency under grant AEI/FEDER, PID2019-107258RB-C32, and also by the Government of Navarre (Dpt. of Economic and Business Development) under grant 0011-1365-2021-000199.

Nordex-Acciona is also gratefully acknowledged for supporting this work with information and data of wind turbines. The open access of this paper has been funded by the Universidad Publica de Navarra.

References

[1] Priya S, Inman DJ. *Energy harvesting technologies*. Springer US; 2009.
[2] Harb A. Energy harvesting: State-of-the-art. Renew Energy 2011;36(10):2641–54. https://doi.org/10.1016/j.renene.2010.06.014.
[3] Wymore ML, van Dam JE, Ceylan H, Qiao D. A survey of health monitoring systems for wind turbines. Renew Sustain Energy Rev 2015. https://doi.org/10.1016/j.rser.2015.07.110.
[4] Oliveira G, Magalhães F, Cunha Á, Caetano E. Continuous dynamic monitoring of an onshore wind turbine. Eng Struct 2018;164(January):22–39. https://doi.org/10.1016/j.engstruct.2018.02.030.
[5] Andrew Swartz R, Lynch JP, Zerbst S, Sweetman B, Rolfes R. Structural monitoring of wind turbines using wireless sensor networks. Smart Struct Syst 2010;6(3):183–96. https://doi.org/10.12989/sss.2010.6.3.183.
[6] De Morais DR, Foschiera LC, Gomes HM. Time and Frequency Domain Analysis of Wind Turbine Towers Under Spatially Correlated Wind Field. Int J Steel Struct 2021;21(6):2028–44. https://doi.org/10.1007/s13296-021-00551-5.
[7] Fan K, et al. A string-suspended and driven rotor for efficient ultra-low frequency mechanical energy harvesting. Energy Convers Manag 2019;198(March):111820. https://doi.org/10.1016/j.enconman.2019.111820.
[8] Graves J, Kuang Y, Zhu M. Counterweight-pendulum energy harvester with reduced resonance frequency for unmanned surface vehicles. Sens Actuators A Phys 2021;321:112577. https://doi.org/10.1016/j.sna.2021.112577.
[9] Li Y, *et al.* Design and experiment of an ultra-low frequency pendulum-based wave energy harvester. *Proceedings of the 14th Annual IEEE International Conference on Nano/Micro Engineered and Molecular Systems, NEMS 2019*, vol. 1; 2019. p. 101–4, doi: 10.1109/NEMS.2019.8915586.
[10] Wu Y, Qiu J, Zhou S, Ji H, Chen Y, Li S. A piezoelectric spring pendulum oscillator used for multi-directional and ultra-low frequency vibration energy harvesting. Appl Energy 2018;231(June):600–14. https://doi.org/10.1016/j.apenergy.2018.09.082.
[11] Wang A, et al. Numerical analysis and experimental study of an ocean wave tetrahedral triboelectric nanogenerator. Appl Energy 2022;307. https://doi.org/10.1016/j.apenergy.2021.118174.
[12] Fan K, Hao J, Wang C, Zhang C, Wang W, Wang F. An eccentric mass-based rotational energy harvester for capturing ultralow-frequency mechanical energy. Energy Convers Manag 2021;241:114301. https://doi.org/10.1016/j.enconman.2021.114301.
[13] O'Donnell R. Energy harvesting from human and machine motion for wireless electronic devices. Proc IEEE 2008;96(9):1455–6. https://doi.org/10.1109/JPROC.2008.927493.
[14] Williams CB, Yates RB. Analysis of a micro-electric generator for microsystems. Sens Actuators A Phys 1996;52(1–3):8–11. https://doi.org/10.1016/0924-4247(96)80118-X.
[15] Mitcheson PD, Yeatman EM, Rao GK, Holmes AS, Green TC. Energy harvesting from human and machine motion for wireless electronic devices. Proc IEEE 2008;96(9):1457–86. https://doi.org/10.1109/JPROC.2008.927494.
[16] Marioli D, Sardini E, Serpelloni M. Electromagnetic Generators Employing Planar Inductors for Autonomous Sensor Applications. Procedia Chem 2009;1(1):469–72. https://doi.org/10.1016/j.proche.2009.07.117.
[17] Wang C, Lai SK, Wang JM, Feng JJ, Ni YQ. An ultra-low-frequency, broadband and multi-stable tri-hybrid energy harvester for enabling the next-generation sustainable power. Appl Energy 2021;291(February):116825. https://doi.org/10.1016/j.apenergy.2021.116825.
[18] Salauddin M, Rasel MS, Kim JW, Park JY. Design and experiment of hybridized electromagnetic-triboelectric energy harvester using Halbach magnet array from handshaking vibration. Energy Convers Manag 2017;153(July):1–11. https://doi.org/10.1016/j.enconman.2017.09.057.
[19] Li Z, Li T, Yang Z, Naguib HE. Toward a 0.33 W piezoelectric and electromagnetic hybrid energy harvester: Design, experimental studies and self-powered applications. Appl Energy 2019;255(April):113805. https://doi.org/10.1016/j.apenergy.2019.113805.
[20] Galchev T, Kim H, Najafi K. Non-resonant bi-stable frequency-increased power scavenger from low-frequency ambient vibration. *TRANSDUCERS 2009 - 15th International Conference on Solid-State Sensors, Actuators and Microsystems*; 2009. p. 632–5. doi: 10.1109/SENSOR.2009.5285404.
[21] Halim MA, Cho H, Park JY. Design and experiment of a human-limb driven, frequency up-converted electromagnetic energy harvester. Energy Convers Manag 2015;106:393–404. https://doi.org/10.1016/j.enconman.2015.09.065.
[22] Ramezanpour R, Nahvi H, Ziaei-Rad S. Electromechanical behavior of a pendulum-based piezoelectric frequency up-converting energy harvester. J Sound Vib 2016;370:280–305. https://doi.org/10.1016/j.jsv.2016.01.052.
[23] Fu H, Theodossiades S, Gunn B, Abdallah I, Chatzi E. Ultra-low frequency energy harvesting using bi-stability and rotary-translational motion in a magnet-tethered oscillator. Nonlinear Dyn 2020;101(4):2131–43. https://doi.org/10.1007/s11071-020-05889-9.
[24] Li M, Deng H, Zhang Y, Li K, Huang S, Liu X. Ultra-low frequency eccentric pendulum-based electromagnetic vibrational energy harvester. Micromachines (Basel) 2020;11(11):1–14. https://doi.org/10.3390/mi11111009.
[25] Fan K, Liu S, Liu H, Zhu Y, Wang W, Zhang D. Scavenging energy from ultra-low frequency mechanical excitations through a bi-directional hybrid energy harvester. Appl Energy 2018;216(January):8–20. https://doi.org/10.1016/j.apenergy.2018.02.086.
[26] Yang F, Zhang J, Lin M, Ouyang S, Qin L. An ultralow frequency, low intensity, and multidirectional piezoelectric vibration energy harvester using liquid as energy-capturing medium. Appl Phys Lett 2020;117(17):pp. https://doi.org/10.1063/5.0022881.
[27] Shen Y, Lu K. Scavenging power from ultra-low frequency and large amplitude vibration source through a new non-resonant electromagnetic energy harvester. Energy Convers Manag 2020;222(June):113233. https://doi.org/10.1016/j.enconman.2020.113233.
[28] Shi G, et al. A piezoelectric vibration energy harvester for multi-directional and ultra-low frequency waves with magnetic coupling driven by rotating balls. Appl Energy 2022;310. https://doi.org/10.1016/j.apenergy.2021.118511.
[29] Miao G, Fang S, Wang S, Zhou S. A low-frequency rotational electromagnetic energy harvester using a magnetic plucking mechanism. Appl Energy 2022;305. https://doi.org/10.1016/j.apenergy.2021.117838.
[30] Yeatman EM. Energy harvesting from motion using rotating and gyroscopic proof masses. Proc Inst Mech Eng C J Mech Eng Sci 2008;222(1):27–36. https://doi.org/10.1243/09544062JMES701.
[31] Pillatsch P, Yeatman EM, Holmes AS. A piezoelectric frequency up-converting energy harvester with rotating proof mass for human body applications. Sens Actuators A Phys 2014;206:178–85. https://doi.org/10.1016/j.sna.2013.10.003.
[32] Li Z, Yan Z, Luo J, Yang Z. Performance comparison of electromagnetic energy harvesters based on magnet arrays of alternating polarity and configuration. *Energy Convers Manag* 2018;179(August):132–40. https://doi.org/10.1016/j.enconman.2018.10.060.
[33] Liu X, Qiu J, Chen H, Xu X, Wen Y, Li P. Design and Optimization of an Electromagnetic Vibration Energy Harvester Using Dual Halbach Arrays. IEEE Trans Magn 2015;51(11):pp. https://doi.org/10.1109/TMAG.2015.2437892.
[34] Halim MA, Rantz R, Zhang Q, Gu L, Yang K, Roundy S. An electromagnetic rotational energy harvester using sprung eccentric rotor, driven by pseudo-walking motion. Appl Energy 2018;217(May):66–74. https://doi.org/10.1016/j.apenergy.2018.02.093.
[35] Cullity CD, Graham BD. Introduction to Magnetic Materials. p. 527–9; 2009.
[36] Bersani AM, Caressa P. Lagrangian descriptions of dissipative systems: a review. Math Mech Solids 2021;26(6):785–803. https://doi.org/10.1177/1081286520971834.
[37] Selesnick I. Total Variation Denoising (An MM Algorithm) [Online].Available: Matrix 2012;2012(2):1–13. http://eeweb.poly.edu/iselesni/lecture_notes/TVDmm/TVDmm.pdf.
[38] van Breugel F, Kutz JN, Brunton BW. Numerical differentiation of noisy data: A unifying multi-objective optimization framework. IEEE Access 2020;8:196865–77. https://doi.org/10.1109/ACCESS.2020.3034077.
[39] Vogel CR. Computational Methods for Inverse Problems. Philadelphia: SIAM; 2002.
[40] Spreemann D, Manoli Y, Folkmer B, Mintenbeck D. Non-resonant vibration conversion. J Micromech Microeng 2006;16(9):S169–73. https://doi.org/10.1088/0960-1317/16/9/S01.
[41] Shen Y, Lu K, Xia Y. "Micro Electromagnetic Vibration Energy Harvester with Mechanical Spring and Iron Frame for Low Frequency Operation", *2018*

International Power Electronics Conference. IPEC-Niigata - ECCE Asia 2018;2018: 2842–7. https://doi.org/10.23919/IPEC.2018.8507500.